Computers & Geosciences 158 (2022) 104953

Contents lists available at ScienceDirect

Computers and Geosciences

journal homepage: www.elsevier.com/locate/cageo

A general and efficient numerical solution of reactive transport with multirate mass transfer

Jingjing Wang [a,b,c,*], Jesus Carrera [b,c], Maarten W. Saaltink [a,c], Cristina Valhondo [b,c,d]

[a] Department of Civil and Environmental Engineering, Universitat Politécnica de Catalunya (UPC), Jordi Girona 1-3, 08034, Barcelona, Spain
[b] Institute of Environmental Assessment and Water Research (IDAEA), Spanish National Research Council (CSIC), c/ Jordi Girona, 20, 08034, Barcelona, Spain
[c] Associated Unit: Hydrogeology Group (UPC-CSIC), Jordi Girona, 08034, Barcelona, Spain
[d] Géosciences Montpellier, Université de Montpellier, CNRS, 300 Avenue Emile Jeanbrau, CC MSE, 34095, Montpellier, France

ARTICLE INFO

Keywords:
Reactive transport modeling
Multirate mass transfer
Kinetic reactions
Non-linear system

ABSTRACT

The presence of low permeability regions within porous media impacts solute transport and the distribution of species concentrations. Therefore, (bio)chemical reactions are equally affected. Multirate Mass Transfer (MRMT) models can be used to represent this anomalous transport process. MRMT conceptualizes the medium as a set of multiple continua: one mobile zone and multiple immobile zones. It simulates species transport in mobile and immobile zones simultaneously, which are related by first-order mass exchange. Numerical modeling of reactive transport in this kind of multicontinua media is complex and demanding because of the high dimensionality of the problem. In this paper, we establish the governing equations of reactive transport in multicontinuum media incorporating chemical kinetics into the governing equations. We propose a general numerical solution of reactive transport with MRMT by applying direct substitution approach (DSA) based on Newton-Raphson method. The efficiency of the proposed algorithm benefits of the block structure of the system, which allows us to eliminate immobile zones equations and leads to significant savings in CPU time. We test the validity of the developed solution by comparison with other numerical and analytical solutions.

1. Introduction

Solute transport is often anomalous in the sense that observed concentrations display numerous non-Fickian features, such as asymmetric spatial distributions or heavy tailed break-through curves (BTCs) (Kosakowski et al., 2001; Zinn et al., 2004; Zhang et al., 2007; Le Borgne and Gouze, 2008). Many methods have been developed to address anomalous transport, including continuous time random walk (CTRW) (Berkowitz and Scher, 1998; Dentz et al., 2004, 2015; Cortis and Berkowitz, 2004), fractional advection-dispersion equations (FADE) (Benson et al., 2000; Schumer et al., 2003; Marseguerra and Zoia, 2008), memory functions (Carrera et al., 1998; Haggerty et al., 2000; Willmann et al., 2008; P. Gouze et al., 2008a), multiple interacting continua (MINC) (Pruess and Narasimhan, 1985; De Dreuzy et al., 2013), structured interacting continua (SINC) (Babey et al., 2015; Rapaport et al., 2017), multirate mass transfer (MRMT) (Haggerty and Gorelick, 1995; Wang et al., 2005; Salamon et al., 2006; Benson and Meerschaert, 2009), and others. These methods are essentially equivalent (Dentz and Berkowitz, 2003; Silva et al., 2009) in that they can be viewed as representing solute mass exchange between a mobile zone and several immobile zones with negligible water velocity. The above references demonstrate that all these methods are relevant for realistic solute transport, which is a pre-condition for realistic reactive transport. But MRMT, MINC and SINC are advantageous because they localize concentrations. That is, concentrations are computed and available at mobile and immobile zones at each point in space, which facilitates reactive calculations. In this study we use MRMT for its simplicity and generality, but our results can be relevant as well for MINC and SINC.

MRMT consists of viewing the medium as the superposition of mobile and immobile zones (Fig. 1a). Typically, the immobile zones represent areas where water does not flow or flows very slowly. Numerous (actually a distribution of) immobile zones are needed to reproduce the distribution of residence time in the immobile regions. Numerical solutions can be viewed as adding extra nodes to every mobile node (Fig. 1b).

MRMT or any other method to address anomalous transport is

* Corresponding author. Department of Civil and Environmental Engineering, Universitat Politécnica de Catalunya (UPC), Jordi Girona 1-3, 08034, Barcelona, Spain.
E-mail address: jingjing.wang@upc.edu (J. Wang).

https://doi.org/10.1016/j.cageo.2021.104953
Received 3 October 2020; Received in revised form 23 September 2021; Accepted 4 October 2021
Available online 23 October 2021

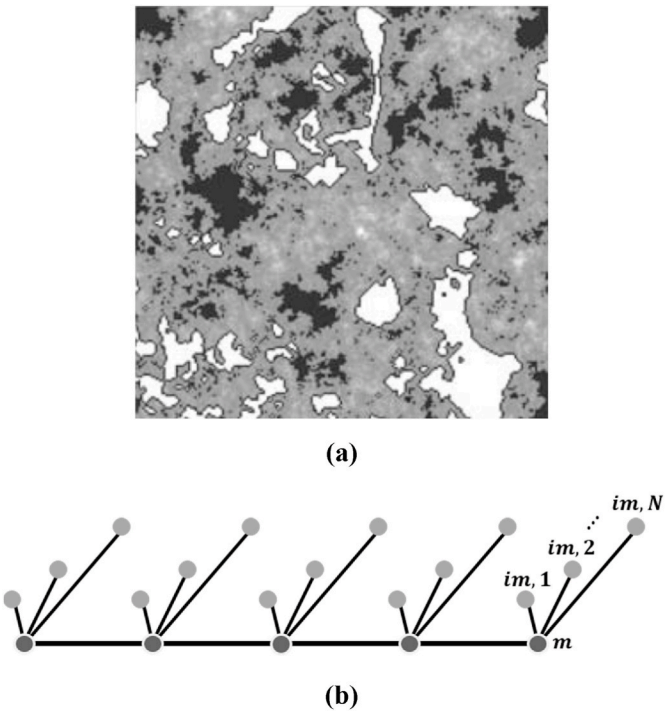

Fig. 1. (a) Illustration of MRMT model in porous media, white areas bounded by black curves represent mobile zone, the black areas represent solid matrix, and the gray areas represent immobile zones, dark gray corresponding to a lower possibility of visit, while light gray denotes a higher possibility to visit (Philippe Gouze et al., 2008b). (b) Numerical discretization of mobile and immobile zones, each circle (labelled m for mobile, and im for immobile) is a node.

relevant for a broad range of reactive transport problems. A clear example is reactive transport in fractured media (see Deng and Spycher, 2019, for a review). Groundwater flow in fractures is much higher than in the rock matrix. Mass transfer between the fracture and the matrix is by molecular diffusion and can lead to mineral-dissolution-precipitation depending on the distance or connection to the fracture. Another important example is mass exchange between pore water and biofilms (e.g., Chen-Charpentier, 1999; Tiwari and Bowers, 2001; Gaebler and Eberl, 2018; Brangarí et al., 2018). Biological reactions mainly take place in biofilms composed of cellular material and extracellular polymeric substances (EPS). As hydraulic conductivity of biofilms is very low, mass transfer is controlled by diffusion and shape and size of the biofilm.

A broad range of residence times may be relevant in many reactive transport problems. Simulating them is relevant not only for proper reproduction of (conservative tracers) breakthrough curves, but also for reproducing geochemical localization (Soler-Sagarra et al., 2016). Localization refers to reactions that occur in some portions of the domain, but which would not occur with the concentrations averaged over all portions of the domain (i.e., in single porosity models). General reactive transport codes must be coupled to MRMT to simulate these problems.

MRMT is computationally costly because it involves multiplying the number of unknowns by the number of immobile zones plus one. This is especially true for implicit solvers, which require building a system of equations with size equal to the number of unknowns. Therefore, it is not surprising that developers have sought "tricks" to reduce this cost. The types of tricks depend on the method. One option is to solve diffusion into the immobile region and then perform a convolution to acknowledge the time variability of concentrations in the mobile zone (Carrera et al., 1998; Wang et al., 2005; Silva et al., 2009). This is tedious, so many others (Haggerty and Gorelick, 1995; Berkowitz et al., 2006, 2008) propose using a Laplace transform, which transforms the convolution into a regular product. But these tricks require that the transport problem is linear. Therefore, they would not be valid for general non-linear reactive transport.

MRMT is still feasible if all reactions are fast (i.e., simulated as equilibrium reactions) and identical because transport of components is linear (Donado et al., 2009; Willmann et al., 2010). However, MRMT is most important for reactive transport problems with kinetic reactions, because of both the broad range of residence times (Haggerty et al., 2000) and chemical localization (Soler-Sagarra et al., 2016).

However, solving MRMT for general reactive transport including kinetics cannot take advantage of the above "tricks". It needs to be solved in the way in Fig. 1b by using general purpose codes, such as PFLOTRAN (Lichtner et al., 2015; Hammond et al., 2014; Iraola et al., 2019), OpenGeoSys (Olaf Kolditz et al., 2012b; O. Kolditz et al., 2012a; Bilke et al., 2019), PHREEQC (Parkhurst and Appelo, 2013), CrunchFlow (Steefel et al., 2015; Beisman et al., 2015), CHEPROO (Bea et al., 2009), Retraso (Saaltink et al., 2004) and PHT3D (Prommer et al., 2001, 2003; Steefel et al., 2015), which is costly. Therefore, it would be desirable to have a general, yet efficient method to solve reactive transport with MRMT.

The objective of this paper is to propose an accurate and efficient numerical approach of MRMT for general reactive transport. In part one, we establish the mathematical governing equations. In part two, we formulate the traditional and proposed numerical solutions. In part three, we verify the accuracy of proposed formulation by comparing with the traditional one and available analytical solutions. We also analyze the efficiency of the proposed algorithm.

2. Governing equations

The immobile zones are fully defined by the distribution of mass exchange rates between mobile and immobile zones. $f(\alpha)$ is the probability density of immobile zones that transfer mass at a given exchange rate α (Haggerty et al., 2000).

The total concentration $\boldsymbol{c}(x,t)$ (i.e., mass of solute per unit volume of medium) at a given point is the weighted sum of mobile $\boldsymbol{c}_m(x,t)$ and immobile $\boldsymbol{c}_{im}(x,\alpha,t)$ concentrations, written as

$$\boldsymbol{c}(x,t) = \varphi_m \boldsymbol{c}_m(x,t) + \varphi_{im} \int_0^\infty f(\alpha)\boldsymbol{c}_{im}(x,\alpha,t)d\alpha \tag{1}$$

where φ_m and φ_{im} are porosity of mobile zone and porosity of immobile zone, respectively. As we deal with reactive transport with several chemical species and reactions, $\boldsymbol{c}$, $\boldsymbol{c}_m$ and $\boldsymbol{c}_{im}$ are vectors containing the concentrations of several species.

The governing mass balance equation to simulate species transport in mobile zone is defined as follows (Willmann et al., 2008)

$$\varphi_m \frac{\partial \boldsymbol{c}_m(x,t)}{\partial t} = L_t[\boldsymbol{c}_m(x,t)] - \varphi_{im} \int_0^\infty \alpha[\boldsymbol{c}_m(x,t) - \boldsymbol{c}_{im}(x,\alpha,t)]f(\alpha)d\alpha + \varphi_m \boldsymbol{r}_m(x,t) \tag{2}$$

where $L_t[\boldsymbol{c}_m(\boldsymbol{x},t)] = -\boldsymbol{q}\nabla\boldsymbol{c}_m + \nabla\cdot(\varphi_m \boldsymbol{D}\nabla\boldsymbol{c}_m)$ is the transport operator, which accounts for advection and dispersion, $\boldsymbol{D}$ is the dispersion and diffusion tensor, $\boldsymbol{q}$ is Darcy flux, $\boldsymbol{r}_m(x,t)$ is a vector of sink-source term that represents the mass added or removed by chemical reactions in mobile zone per unit volume of water per unit time.

Mass in immobile zones exchange with the mobile zone as

$$\frac{\partial \boldsymbol{c}_{im}(x,\alpha,t)}{\partial t} = \alpha[\boldsymbol{c}_m(x,t) - \boldsymbol{c}_{im}(x,\alpha,t)] + \boldsymbol{r}_{im}(x,\alpha,t) \tag{3}$$

Different distributions can be used for the mass exchange rate α. The (truncated-) power law distribution (Haggerty et al., 2000, 2002; Schumer et al., 2003; Benson and Meerschaert, 2009) is commonly used.

Integrating equation *(3)* with weight $f(\alpha)$ in terms of $d\alpha$, and multiplying by φ_{im}, then adding it into equation *(2)*, yields the governing equation for the total concentrations,

$$\varphi_m \frac{\partial \boldsymbol{c}_m(x,t)}{\partial t} + \varphi_{im} \int_0^\infty f(\alpha) \frac{\partial \boldsymbol{c}_{im}(x,\alpha,t)}{\partial t} d\alpha = L_t[\boldsymbol{c}_m(x,t)] + \boldsymbol{r}(x,t) \tag{4}$$

in which, $\boldsymbol{r}(x,t)$ is the total reaction rate (now per unit volume of porous medium) that integrates reaction in both mobile and immobile zones,

$$\boldsymbol{r}(x,t) = \varphi_m \boldsymbol{r}_m(x,t) + \varphi_{im} \int_0^\infty f(\alpha) \boldsymbol{r}_{im}(x,\alpha,t) d\alpha \tag{5}$$

For any chemical system, reaction rates $\boldsymbol{r}(x,t)$ at any point can be written as,

$$\boldsymbol{r}(x,t) = \boldsymbol{S}_e^T \boldsymbol{r}_e(x,t) + \boldsymbol{S}_k^T \boldsymbol{r}_k(x,t) \tag{6}$$

where $\boldsymbol{S}_e$ and $\boldsymbol{S}_k$ are the stoichiometric matrices describing equilibrium and kinetic reactions respectively, $\boldsymbol{r}_e$ and $\boldsymbol{r}_k$ represent the vectors of reaction rates (Saaltink et al., 1998).

The component matrix $\boldsymbol{U}$ is introduced to eliminate equilibrium reactions in equation *(6)*, and to reduce the number of unknowns (Saaltink et al., 1998; Molins et al., 2004). $\boldsymbol{U}$ is the kernel of $\boldsymbol{S}_e^T$, satisfying $\boldsymbol{U}\boldsymbol{S}_e^T = 0$. Multiply equation *(2)* and *(3)* by component matrix $\boldsymbol{U}$, we obtain the simplified governing equation in terms of components that is written as,

$$\varphi_m \frac{\partial \boldsymbol{u}_m(x,t)}{\partial t} = L_t[\boldsymbol{u}_m(x,t)] - \varphi_{im} \int_0^\infty \alpha[\boldsymbol{u}_m(x,t) - \boldsymbol{u}_{im}(x,\alpha,t)] f(\alpha) d\alpha + \varphi_m \boldsymbol{U}\boldsymbol{S}_k^T \boldsymbol{r}_{k,m}(x,t) \tag{7}$$

$$\frac{\partial \boldsymbol{u}_{im}(x,\alpha,t)}{\partial t} = \alpha[\boldsymbol{u}_m(x,t) - \boldsymbol{u}_{im}(x,\alpha,t)] + \boldsymbol{U}\boldsymbol{S}_k^T \boldsymbol{r}_{k,im}(x,\alpha,t) \tag{8}$$

where component vector $\boldsymbol{u} = \boldsymbol{U}\boldsymbol{c}$ is the product of component matrix and concentration vector.

2.1. Numerical equations

We solve the non-linear coupled reactive transport governing equation *(7)* and *(8)* by applying Newton-Raphson method, i.e., direct substitution approach (DSA) (Steefel and Lasaga, 1994; Saaltink et al., 1998, 2001; Molins et al., 2004; Liu et al., 2019). Therefore, we define the system equations in both mobile and immobile zones simultaneously. The details are given in Appendix A. To explain the algorithm, we write the equation system in the form $\boldsymbol{g}(\boldsymbol{x}) = 0$:

$$\boldsymbol{g}_m = \varphi_m \frac{\partial \boldsymbol{u}_m(x,t)}{\partial t} - L_t[\boldsymbol{u}_m(x,t)] + \sum_{j=1}^{N} \boldsymbol{F}_j - \varphi_m \boldsymbol{U}\boldsymbol{S}_k^T \boldsymbol{r}_m(x,t) = 0 \tag{9}$$

$$\boldsymbol{g}_{im,j} = \frac{\partial \boldsymbol{u}_{im,j}(x,t)}{\partial t} - \alpha_j \left[\boldsymbol{u}_m(x,t) - \boldsymbol{u}_{im,j}(x,t)\right] - \boldsymbol{U}\boldsymbol{S}_k^T \boldsymbol{r}_{im,j}(x,t) = 0, j = 1, \cdots, N \tag{10}$$

where N is the number of immobile zones for each nodes and $\boldsymbol{F}_j$ is the exchange rate between mobile and immobile zone.

The Newton-Raphson method is based on solving the linearized form of the equations, i.e.,

$$\boldsymbol{g}^{i+1} = \boldsymbol{g}(\boldsymbol{x}^{i+1}) \approx \boldsymbol{g}(\boldsymbol{x}^i) + \frac{\partial \boldsymbol{g}(\boldsymbol{x})}{\partial \boldsymbol{x}} (\boldsymbol{x}^{i+1} - \boldsymbol{x}^i) = 0 \tag{11}$$

In our case, this can be written as,

$$\begin{bmatrix} \left(\frac{\partial \boldsymbol{g}_m}{\partial \boldsymbol{u}_m^{k+1}}\right)^i & \left(\frac{\partial \boldsymbol{g}_m}{\partial \boldsymbol{u}_{im,1}^{k+1}}\right)^i & \cdots & \left(\frac{\partial \boldsymbol{g}_m}{\partial \boldsymbol{u}_{im,N}^{k+1}}\right)^i \\ \left(\frac{\partial \boldsymbol{g}_{im,1}}{\partial \boldsymbol{u}_m^{k+1}}\right)^i & \left(\frac{\partial \boldsymbol{g}_{im,1}}{\partial \boldsymbol{u}_{im,1}^{k+1}}\right)^i & \cdots & 0 \\ \vdots & \vdots & \ddots & \vdots \\ \left(\frac{\partial \boldsymbol{g}_{im,N}}{\partial \boldsymbol{u}_m^{k+1}}\right)^i & 0 & \cdots & \left(\frac{\partial \boldsymbol{g}_{im,N}}{\partial \boldsymbol{u}_{im,N}^{k+1}}\right)^i \end{bmatrix} \begin{bmatrix} \left(\boldsymbol{u}_m^{k+1}\right)^{i+1} - \left(\boldsymbol{u}_m^{k+1}\right)^i \\ \left(\boldsymbol{u}_{im,1}^{k+1}\right)^{i+1} - \left(\boldsymbol{u}_{im,1}^{k+1}\right)^i \\ \vdots \\ \left(\boldsymbol{u}_{im,N}^{k+1}\right)^{i+1} - \left(\boldsymbol{u}_{im,N}^{k+1}\right)^i \end{bmatrix} = - \begin{bmatrix} \left(\boldsymbol{g}_m\right)^i \\ \left(\boldsymbol{g}_{im,1}\right)^i \\ \vdots \\ \left(\boldsymbol{g}_{im,N}\right)^i \end{bmatrix} \tag{12}$$

in which, $\boldsymbol{u}_m$ is the column vector containing all components in mobile zone at all nodes, and $\boldsymbol{u}_{im,j}$ is the column vector containing all the components in jth immobile zone at all nodes, the matrix at the left hand side is the Jacobian matrix $(\partial \boldsymbol{g}/\partial \boldsymbol{u}^{k+1})^i$ consisting of the derivatives of system equations with respect to the unknown components in both mobile and immobile zones at all nodes.

The important feature of equation *(12)* is the block diagonal form of the lower portion of the Jacobian, which allows us to rewrite it into blocks representing the mobile and immobile zones separately and leads to

$$\begin{bmatrix} \boldsymbol{A} & \boldsymbol{B} \\ \boldsymbol{C} & \boldsymbol{D} \end{bmatrix} \begin{bmatrix} \boldsymbol{x} \\ \boldsymbol{y} \end{bmatrix} = \begin{bmatrix} \boldsymbol{a} \\ \boldsymbol{b} \end{bmatrix} \tag{13}$$

Block $\boldsymbol{D}$ is a block diagonal matrix with $N_n \times N$ blocks of size $N_u \times N_u$ (N_n being the number of mesh nodes and N_u the number of components). This characteristic can be used to solve system equations by defining Schur complement of block $\boldsymbol{D}$, that is $\boldsymbol{A} - \boldsymbol{B}\boldsymbol{D}^{-1}\boldsymbol{C}$. In this way, solutions can be efficiently solved by

$$\left(\boldsymbol{A} - \boldsymbol{B}\boldsymbol{D}^{-1}\boldsymbol{C}\right)\boldsymbol{x} = \left(\boldsymbol{a} - \boldsymbol{B}\boldsymbol{D}^{-1}\boldsymbol{b}\right) \tag{14}$$

$$\boldsymbol{y} = \boldsymbol{D}^{-1}(\boldsymbol{b} - \boldsymbol{C}\boldsymbol{x}) \tag{15}$$

The traditional approach is to solve equation (12) as one large system with a size equal to $N_n \times N_u \times N$. We propose to split the solution into two parts, first solving equation (15), followed by equation (14). We conjecture that this is much less costly, because equation (14) is N times smaller than that of the traditional approach of equation (12) and, because the block diagonal structure of matrix $\boldsymbol{D}$ permits the calculation of its inverse for each immobile zone of each node separately. The approach is valid not only for MRMT, but also for MINC of SINC. The difference lies in that, if these methods are adopted, then matrix $\boldsymbol{D}$ must include all immobile zones connected to a node, instead of each immobile zone separately. Note that both solution approaches are mathematically equivalent, which means that the convergence of the Newton-Rapson method will be identical for both.

2.2. Algorithm

We apply two nested Newton-Raphson iteration loops to solve the nonlinear system in each time step, the outside one is used to solve components transport, the inner one is used for chemical speciation calculation in each iteration. The algorithm proceeds as follows:

Step 0 Set $i = 0$, and initialize components $(\boldsymbol{u}^{k+1})^i = 0$.
Step 1 Compute functions $\boldsymbol{g}^i$.

Step 2 Compute the derivative of functions to construct Jacobian matrix $\left(\frac{\partial g}{\partial u^{k+1}}\right)^i$.

Step 3 Solve system equation (14) and (15) to get solutions $\Delta u^{k+1} = (u^{k+1})^{i+1} - (u^{k+1})^i$.

Step 4 Compute solutions at next iteration step, $(u^{k+1})^{i+1} = (u^{k+1})^i + \Delta u^{k+1}$.

Step 5 Execute speciation calculation of primary species concentrations $(c_1^{k+1})^i$ and secondary species concentrations $(c_2^{k+1})^i$ from components $(u^{k+1})^i$ according to equations of components and mass action law iteratively. Then calculate the derivatives of $\left(\frac{\partial r(u^{k+1})}{\partial c_1^{k+1}}\right)^i$ and $\left(\frac{\partial c_1^{k+1}}{\partial u^{k+1}}\right)^i$. Furthermore, compute the derivatives of kinetics with respect to components $\left(\frac{\partial r_{k,m}^{k+1}}{\partial u_m^{k+1}}\right)^i$ and $\left(\frac{\partial r_{k,im,j}^{k+1}}{\partial u_{im,j}^{k+1}}\right)^i$ to facilitate the calculation of function derivatives $\left(\frac{\partial g}{\partial u^{k+1}}\right)^i$.

Step 6 Convergence check. If $(u^{k+1})^{i+1}$ close to $(u^{k+1})^i$ or $g^{i+1} \approx 0$, then stop. Otherwise, set $i = i + 1$, and return to step 1.

3. Accuracy verification and efficiency analysis

3.1. Accuracy verification

To test the accuracy of the proposed solution, we perform 1D simulations of (1) non-reactive transport test, (2) multicomponent reactive transport for MRMT in chemical equilibrium and (3) kinetics. All these models are under the same MRMT model, with $L = 100.0$ m, $\varphi_m = 0.1$, $\varphi_{im} = 0.1$, $q = 1.0$m/s, $D = 10.0$m^2/s, and a power law distribution of mass exchange rates, the corresponding residence time (that is the inverse of the mass exchange rate, $\tau \equiv 1/\alpha$) distribution, $P(\tau) \propto \tau^{-\beta}$, with exponent $\beta = 3/2$. Parameters to generate the simulations are shown in Table 1.

3.1.1. Non-reactive solute

We compared our method with that of Silva et al. (2009), which differs from our method in that it writes the concentrations of the immobile zones as an explicit function of those of the mobile zones. This can be done only for non-reactive transport. In Fig. 2, the break-through curve of solute at distance $x = 100.0$ m is displayed. It is a typical BTC, the characteristic advection time t_{adv} is between $\varphi_m x/q$ and $(\varphi_m + \varphi_{im})x/q$, and the concentrations decrease for times longer than the characteristic advection time, at the late times the power law tail is reproduced as $c(t) \propto t^{-\beta-1}$. The blue solid line is the numerical formulation proposed by Silva et al. (2009), and the square red line is the numerical solution of our proposed method. As can be seen, these two numerical solutions are almost identical. The small differences may be due to the explicit calculation of the concentrations of the immobile zones by the method of Silva et al. (2009).

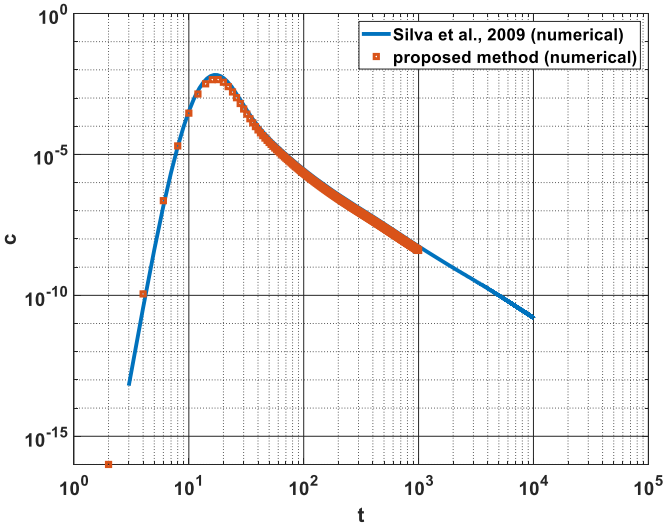

Fig. 2. Comparison between the results of the non-reactive transport model calculated by the proposed method and the method of Silva et al. (2009).

3.1.2. Equilibrium gypsum dissolution

Fig. 3 displays component (left) concentrations and (right) reaction rates for a case physically identical to the above one, but transporting Ca^{2+} and SO_4^{2-} in equilibrium with gypsum $CaSO_4 = Ca^{2+} + SO_4^{2-}$ for which we apply the mass action law: $a_{Ca^{2+}} a_{SO_4^{2-}} = K$, where a is activity and K is an equilibrium constant ($logK(25°C) = -4.4823$). Activities are calculated from concentrations by means of the extended Debye Hückel equation. We compare the numerical results of our proposed method with the analytical solution of Donado et al. (2009). As we can see the numerical results are consistent with analytical solutions. A clear separation between BTCs in mobile and immobile zones is presented due to the physical mass transfer limitations, components both in mobile and immobile zones are retarded at late time. Notice that the reaction rates are negative, that means calcium ion and sulfate ion are oversaturated and precipitated into gypsum. The analytical solutions of reaction rates in mobile and immobile zones, which are given by

$$\boldsymbol{r}_{im}(x,t) = \int_0^\infty f(\alpha)\left\{\frac{\partial \boldsymbol{c}_{im}(x,\alpha,t)}{\partial t} - \alpha[\boldsymbol{c}_m(x,t) - \boldsymbol{c}_{im}(x,\alpha,t)]\right\} d\alpha \tag{16}$$

Table 1
The distribution of mass exchange rates α_j and the corresponding probabilities p_j of each immobile zone.

j	α_j	p_j	j	α_j	p_j	j	α_j	p_j	j	α_j	p_j
1	0.0001	0.001477	15	0.0060	0.002310	29	0.2000	0.040520	43	7.0	0.033709
2	0.0002	0.001306	16	0.0070	0.002136	30	0.3000	0.032091	44	8.0	0.028505
3	0.0003	0.001045	17	0.0080	0.001997	31	0.4000	0.027333	45	9.0	0.024302
4	0.0004	0.000899	18	0.0090	0.001881	32	0.5000	0.024131	46	10.0	0.067106
5	0.0005	0.000801	19	0.0100	0.008293	33	0.6000	0.021774	47	20.0	0.071496
6	0.0006	0.000730	20	0.0200	0.013035	34	0.7000	0.019938	48	30.0	0.020411
7	0.0007	0.000676	21	0.0300	0.010420	35	0.8000	0.018453	49	40.0	0.006370
8	0.0008	0.000631	22	0.0400	0.008956	36	0.9000	0.017217	50	50.0	0.002072
9	0.0009	0.000595	23	0.0500	0.007979	37	1.0	0.072141	51	60.0	0.000691
10	0.0010	0.002626	24	0.0600	0.007265	38	2.0	0.108071	52	70.0	0.000234
11	0.0020	0.004129	25	0.0700	0.006713	39	3.0	0.077997	53	80.0	0.000080
12	0.0030	0.003303	26	0.0800	0.006270	40	4.0	0.060633	54	90.0	0.000027
13	0.0040	0.002842	27	0.0900	0.005903	41	5.0	0.048885	55	100.0	0.000014
14	0.0050	0.002534	28	0.1000	0.025896	42	6.0	0.040293			

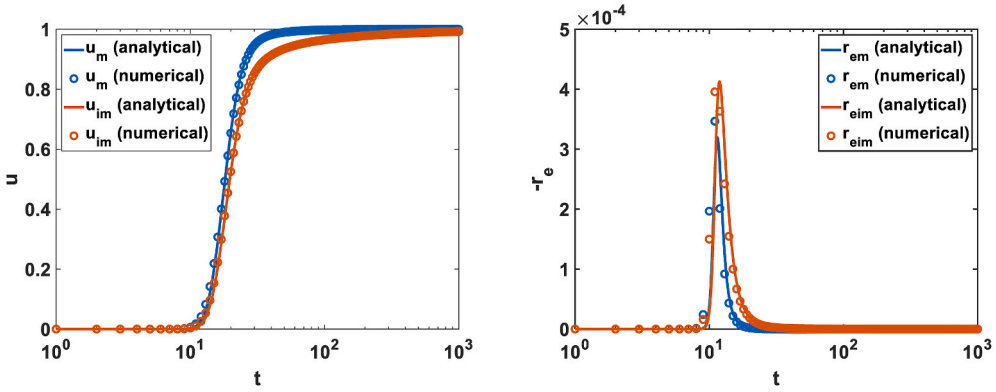

Fig. 3. Distribution of (left) components u_m and u_{im}, (right) reaction rates r_m and r_{im} versus time at distance $x = 100.0$m. The blue color represents state variables in the mobile zone, and the red color represents state variables in immobile zones. The solid lines are the analytical solutions and the circle dot lines are the proposed numerical solutions. (For interpretation of the references to color in this figure legend, the reader is referred to the Web version of this article.)

$$\boldsymbol{r}_m(x,t) = -\frac{\partial \boldsymbol{c}_{m,2}(x,t)}{\partial \boldsymbol{u}_m(x,t)}\left[\frac{\varphi_{im}}{\varphi_m}\int_0^\infty f(\alpha)\frac{\partial \boldsymbol{u}_{im}(x,\alpha,t)}{\partial t}d\alpha\right] + \frac{\varphi_{im}}{\varphi_m}\int_0^\infty f(\alpha)\frac{\partial \boldsymbol{c}_{im,2}(x,\alpha,t)}{\partial \boldsymbol{u}_{im}(x,\alpha,t)}\frac{\partial \boldsymbol{u}_{im}(x,\alpha,t)}{\partial t}d\alpha - \frac{\partial^2 \boldsymbol{c}_{m,2}(x,t)}{\partial \boldsymbol{u}_m^2(x,t)}\nabla^T \boldsymbol{u}_m(x,t)\boldsymbol{D}\nabla \boldsymbol{u}_m(x,t) - \frac{\varphi_{im}}{\varphi_m}\boldsymbol{r}_{im}(x,t) \tag{17}$$

3.1.3. Kinetic reaction

To test the performance of our proposed solution in chemical kinetics, we choose a simple first-order kinetics. In this case, the analytical solution can be found in the Laplace domain (the solution is deduced in Appendix B). Then we simulate the distribution of components and kinetic rates both in mobile and immobile zones over time with the component degradation rate $\kappa = 0.01$. As we can see the proposed numerical solutions agree with the analytical solution as displayed in Fig. 4. Comparing the evolution of components in chemical equilibrium (Fig. 4 left), the presence of chemical reactions decreases the concentrations of the components both in mobile and immobile zones.

3.2. Efficiency analysis

The efficiency of the algorithm depends on the problem size n, the total number of unknowns of system equation (13) that equals to the number of mesh nodes times the number of components times the number of immobile zones plus one. In our problem, the matrix operation is the most time consuming. Both the computational cost of matrix multiplication and matrix inversion are $O(n^3)$.

Instead of solving system equation (13) globally, we solve it in blocks representing mobile and immobile zones separately, using equations (14) and (15). Since these two approaches are mathematically identical, the two will converge to the same solution within the same iterations. The advantage of the proposed block solution is that it reduces the size of the system to be the number of mesh nodes times the number of components.

We simulate an irreversible bimolecular reaction $A + B \rightarrow C$for the number of immobile zones equal to 3, 10, 30, 50, 70 and 100, with a second-order kinetics $r_k = \kappa c_A c_B$. In Fig. 5, we compare the CPU time of the proposed method (i.e., block solver) and full DSA on a log-log scale. As we can see, the CPU time of the block solver increases linearly with the number of immobile zones (N), while that of the full DSA increases much faster, approximating to N^3. Clearly, the block solver runs faster than full DSA for a higher number of immobile zones. For a small number of immobile zones, the full DSA runs faster because of the costs of building the more complicated structure of the block solver.

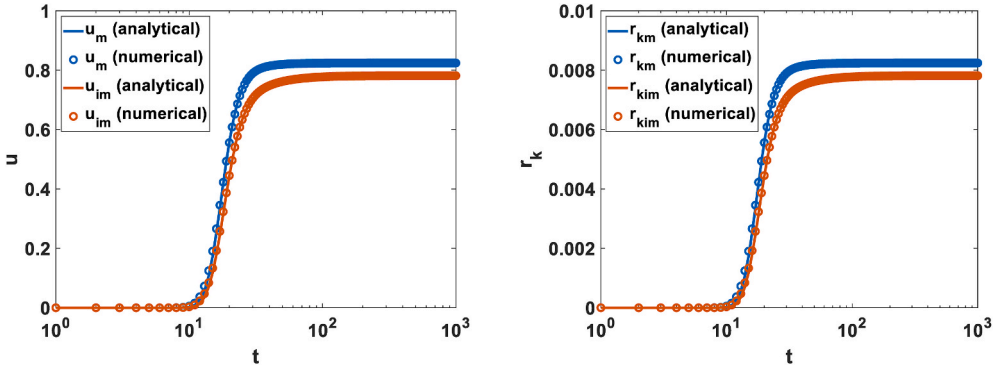

Fig. 4. Distribution of (left) components u_m and u_{im}, (right) reaction rates r_m and r_{im} versus time at distance $x = 100.0$m. The blue color represents state variables in the mobile zone, and the red color represents state variables in immobile zones. The solid lines are the analytical solutions and the circle dot lines are the proposed numerical solutions. (For interpretation of the references to color in this figure legend, the reader is referred to the Web version of this article.)

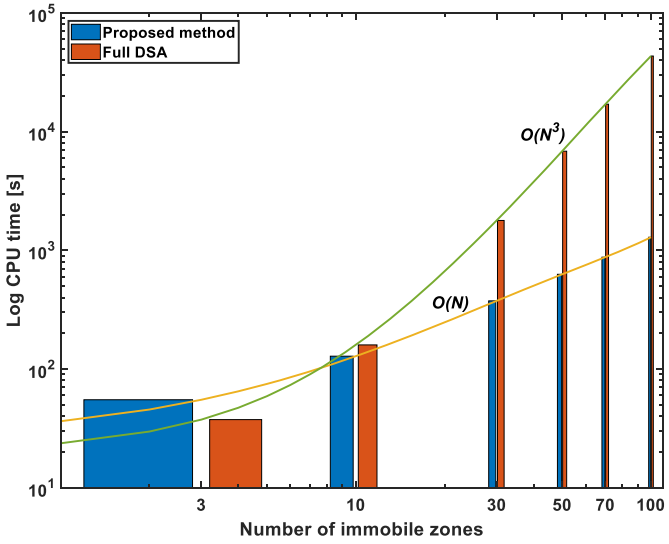

Fig. 5. CPU time comparison between proposed method and full DSA for different number of immobile zones. The chemical systems are identical for all cases that is an irreversible bimolecular reaction $A + B \rightarrow C$, with a second-order kinetics $r_k = \kappa c_A c_B$.

4. Conclusions

The proposed method is effective and efficient for reactive transport modeling capable of accounting for numerous immobile zones. We formulate the general numerical solution of reactive transport with MRMT based on the Newton-Raphson method, which enables us to simulate complex chemical kinetics. For chemical systems, whatever it is in equilibrium or in kinetics, the convergent solution is efficiently solved within several iterations.

The proposed numerical solution is verified in case of passive solute transport, chemical equilibrium and chemical kinetics. In all cases the simulations agree very well with available analytical solutions and other numerical solutions. The full consistency between the proposed numerical solutions and available analytical solutions indicate that our proposed method is capable of reproducing the anomalous transport of reactive transport with MRMT.

The computational efficiency of the proposed algorithm is improved by solving system equations in block instead of full DSA, which eliminates the impact of the number of immobile zones on the computational complexity and decreases the size of the linear system to be the number of mesh nodes times the number of components. This may become particularly important for more complicated chemical models in combination with MRMT. In that case the full DSA can become prohibitively expensive in CPU and the block solver may be the only feasible method.

The advantage of the method increases with the number of immobile zones. Babey et al. (2015) concluded that five immobile zones (compared to one hundred in our models) are sufficient to address anomalous transport of non-reactive solutes. However, this may be different for reactive transport because of the broad range of residence times (Haggerty et al., 2000) and chemical localization (Soler-Sagarra et al., 2016). The number of immobile zones needed for proper reproduction of reactive processes requires further research.

Computer code availability

Name of code: Reactive Transport with Multirate Mass Transfer.

Developer: Jingjing Wang.

Contact detail: Department of Civil and Environmental Engineering, Universitat Politécnica de Catalunya (UPC), Jordi Girona 1-3, 08034 Barcelona, Spain.

Email: jingjing.wang.xiang@gmail.com.

Year first available: October 2020.

Hardware required: No specific hardware is required. However, the code has been developed on a computer with processor Intel® Core™ i5-6500 CPU @ 3.20 GHz, 16 GB Installed memory (RAM), 64-bit Operating System, x64-based processor.

Software development platform: Microsoft Visual Studio 2015.

Program language: object-oriented programming FORTRAN 2003.

Compiler: Intel Parallel Studio XE 2017 Cluster Edition for Windows*

Library: Intel® Math Kernel Library. To solve the system equation *(14)*, we call routine dgbtrf() to compute the LU factorization of the left hand side matrix of system equation *(14)*, then we call routine dgbtrs() to solve the linear system with the LU-factored square coefficient matrix returned by routine dgbtrf().

Program size: 4.39 MB.

Details on how to access the open-source code: the source code can be freely download from GitHub on the public repository https://github.com/Jingjingwangxiang/RT_MRMT_DSA.

Our codes are developed in object-oriented instead of procedural-oriented which lacks flexibility and extensibility (Meysman et al., 2003a, 2003b; Meysman et al., 2003b). The object-oriented programming allows the code reusability and facilitates the implementation of reactive transport modeling. To simulate the reactions, two main modules are developed. The biochemical system module simulates the localized chemical reactions occurring in a (bio)chemical system, it contains procedures that are capable of constructing the stoichiometric matrix and component matrix. The local biochemistry module captures (bio)chemical state variables at each mesh node, such as components, concentrations, equilibrium reaction rates, kinetics, as well as the derivatives of kinetics with respect to concentrations, etc. It encapsulates procedures of chemical calculations that are capable of computing the state variables at each mesh node by using the biochemistry system module. These two main developed modules are coupled with the transport equations in the reactive transport module, which enables the modeling of reactive transport.

Authorship contributions statement

Jingjing Wang: Conceptualization, Methodology, Code Programming, Investigation, Writing - original draft, Writing, review & editing,

Jesus Carrera: Conceptualization, Supervision, Writing, reviewing & editing,

Maarten W. Saaltink: Conceptualization, Methodology, Supervision, Writing, review & editing.

Cristina Valhondo: Supervision, Writing, review & editing.

Declaration of competing interest

The authors declare that they have no known competing financial interests or personal relationships that could have appeared to influence the work reported in this paper.

Acknowledgements

The authors acknowledge the support of project NITREM initiated and funded by EIT (European Institute of Innovation and Technology), and the Water-JPI European Union project MARadentro, project number PCI2019-103425-WW2017.

Appendix A. Numerical discretization of governing equations

In practice, MRMT model is substituted by a finite number of immobile zones. In this way, the continuous governing equation *(7)* and *(8)* are discretized as follows,

$$\varphi_m \frac{\partial \boldsymbol{u}_m(x,t)}{\partial t} = L_t[\boldsymbol{u}_m(x,t)] - \sum_{j=1}^{N} \boldsymbol{F}_j + \varphi_m \boldsymbol{R}_m(x,t) \tag{A1}$$

$$\boldsymbol{F}_j = \varphi_{im,j}\alpha_j\left[\boldsymbol{u}_m(x,t) - \boldsymbol{u}_{im,j}(x,t)\right] \tag{A2}$$

$$\boldsymbol{R}_m(x,t) = \boldsymbol{U}\boldsymbol{S}_k^T \boldsymbol{r}_{k,m}(\boldsymbol{u}_m(x,t)) \tag{A3}$$

$$\frac{\partial \boldsymbol{u}_{im,j}(x,t)}{\partial t} = \alpha_j\left[\boldsymbol{u}_m(x,t) - \boldsymbol{u}_{im,j}(x,t)\right] + \boldsymbol{R}_{im,j}(x,t),\ j = 1,\ \cdots,\ N \tag{A4}$$

$$\boldsymbol{R}_{im,j}(x,t) = \boldsymbol{U}\boldsymbol{S}_k^T \boldsymbol{r}_{k,im,j}\left(\boldsymbol{u}_{im,j}(x,t)\right) \tag{A5}$$

where $\boldsymbol{F}_j$ is the mass exchange between mobile and jth immobile zone, $\varphi_{im,j} = \varphi_{im}p_j$ is the weighted porosity in jth immobile zone, p_j is the probability for mass exchange rate α_j accounting in the jth immobile zone, N is the number of immobile zones.

To obtain the numerical discretization of the system equations, a forward finite difference method is used to discretize the first derivative in time, and the finite element method is applied to discretize the governing partial difference equations. Meanwhile, state variables are evaluated at some time between time step k and $k+1$.

The resulting discretized system equations are given below,

$$(\boldsymbol{g}_m)^i = \left(\frac{\boldsymbol{G}}{\Delta t} + \theta_t \boldsymbol{E}\right)\left(\boldsymbol{u}_m^{k+1}\right)^i - \left(\frac{\boldsymbol{G}}{\Delta t} - (1-\theta_t)\boldsymbol{E}\right)\boldsymbol{u}_m^k + \frac{\boldsymbol{G}}{\varphi_m}\sum_{j=1}^{N}\left(\boldsymbol{F}_j^{k+\theta_t}\right)^i - \boldsymbol{G}\left(\boldsymbol{R}_m^{k+\theta_r}\right)^i = 0 \tag{A6}$$

$$\left(\boldsymbol{g}_{im,j}\right)^i = \frac{\left(\boldsymbol{u}_{im,j}^{k+1}\right)^i - \boldsymbol{u}_{im,j}^k}{\Delta t} - \alpha_j\left[\left(\boldsymbol{u}_m^{k+\theta_t}\right)^i - \left(\boldsymbol{u}_{im,j}^{k+\theta_t}\right)^i\right] - \left(\boldsymbol{R}_{im,j}^{k+\theta_r}\right)^i = 0,\ j = 1,\ \cdots,\ N \tag{A7}$$

in which, $\boldsymbol{E}$ is the global matrix accounting for advection and dispersion, $\boldsymbol{G}$ is the global matrix that assembles porosity in the mobile zone, i is the iteration number at each time step, $\theta_t \in [0,\ 1]$ is a temporal weight factor for transport, and $\theta_r \in [0,\ 1]$ is a weight factor for kinetics.

The entries of Jacobian matrix are formulated as follows,

$$\left(\frac{\partial \boldsymbol{g}_m}{\partial \boldsymbol{u}_m^{k+1}}\right)^i = \left(\frac{\boldsymbol{G}}{\Delta t} + \boldsymbol{E}\theta\right) \otimes \boldsymbol{I}_{N_u} + (\boldsymbol{G}/\varphi_m)\sum_{j=1}^{N}\varphi_{im,j}\alpha_j\theta_t \boldsymbol{I}_{N_n} \otimes \boldsymbol{I}_{N_u} - \boldsymbol{G}\theta_r\left(\frac{\partial \boldsymbol{R}_m^{k+1}}{\partial \boldsymbol{u}_m^{k+1}}\right)^i \tag{A8}$$

$$\left(\frac{\partial \boldsymbol{g}_m}{\partial \boldsymbol{u}_{im,j}^{k+1}}\right)^i = -\varphi_{im,j}\alpha_j\theta_t(\boldsymbol{G}/\varphi_m)\boldsymbol{I}_{N_n} \otimes \boldsymbol{I}_{N_u} \tag{A9}$$

$$\left(\frac{\partial \boldsymbol{g}_{im,j}}{\partial \boldsymbol{u}_m^{k+1}}\right)^i = -\alpha_j\,\theta_t \boldsymbol{I}_{N_n} \otimes \boldsymbol{I}_{N_u} \tag{A10}$$

$$\left(\frac{\partial \boldsymbol{g}_{im,j}}{\partial \boldsymbol{u}_{im,j}^{k+1}}\right)^i = \left(\frac{1}{\Delta t} + \alpha_j\theta_t\right)\boldsymbol{I}_{N_n} \otimes \boldsymbol{I}_{N_u} - \theta_r\left(\frac{\partial \boldsymbol{R}_{im,j}^{k+1}}{\partial \boldsymbol{u}_{im,j}^{k+1}}\right)^i \tag{A11}$$

in which, N_n is the number of mesh nodes, N_u is the number of components, $\otimes$ represents Kronecker product, $\boldsymbol{I}_{N_n}$ and $\boldsymbol{I}_{N_u}$ are identity matrix with dimensions equal to $N_n \times N_n$ and $N_u \times N_u$, respectively.

The derivatives of reaction rates with respect to components at each node are calculated according to the chain rule, that is

$$\left(\frac{\partial \boldsymbol{R}_m^{k+1}}{\partial \boldsymbol{u}_m^{k+1}}\right)^i = \boldsymbol{U}\boldsymbol{S}_K^T\left(\frac{\partial \boldsymbol{r}_{k,m}^{k+1}}{\partial \boldsymbol{u}_m^{k+1}}\right)^i = \boldsymbol{U}\boldsymbol{S}_K^T\left(\frac{\partial \boldsymbol{r}_{k,m}^{k+1}}{\partial \boldsymbol{c}_{1m}^{k+1}}\right)^i\left[\left(\frac{\partial \boldsymbol{u}_m^{k+1}}{\partial \boldsymbol{c}_{1m}^{k+1}}\right)^i\right]^{-1} \tag{A12}$$

$$\left(\frac{\partial \boldsymbol{R}_{im,j}^{k+1}}{\partial \boldsymbol{u}_{im,j}^{k+1}}\right)^i = \boldsymbol{U}\boldsymbol{S}_K^T\left(\frac{\partial \boldsymbol{r}_{k,im,j}^{k+1}}{\partial \boldsymbol{u}_{im,j}^{k+1}}\right)^i = \boldsymbol{U}\boldsymbol{S}_K^T\left(\frac{\partial \boldsymbol{r}_{k,im,j}^{k+1}}{\partial \boldsymbol{c}_{1im,j}^{k+1}}\right)^i\left[\left(\frac{\partial \boldsymbol{u}_{im,j}^{k+1}}{\partial \boldsymbol{c}_{1im,j}^{k+1}}\right)^i\right]^{-1} \tag{A13}$$

both are matrices of size $N_u \times N_u$.

Appendix B. Analytical solution of reactive transport in multicontinuum media for first-order kinetics in the Laplace Domain

For a chemical system satisfies $\boldsymbol{U}\boldsymbol{S}_k^T\boldsymbol{r}_{k,m}(x,t) = -\boldsymbol{r}_{k,m}(x,t)$, $\boldsymbol{U}\boldsymbol{S}_k^T\boldsymbol{r}_{k,im}(x,\alpha,t) = -\boldsymbol{r}_{k,im}(x,\alpha,t)$, and the chemical kinetics follows first-order decay, $\boldsymbol{r}_{k,m}(x,t) = \kappa\boldsymbol{u}_m(x,t)$, $\boldsymbol{r}_{k,im}(x,\alpha,t) = \kappa\boldsymbol{u}_{im}(x,\alpha,t)$, then the governing equation *(7)* and *(8)* in mobile and immobile domains simplify to be linear, that is,

$$\varphi_m \frac{\partial \boldsymbol{u}_m(x,t)}{\partial t} = L_t[\boldsymbol{u}_m(x,t)] - \varphi_{im} \int_0^\infty \alpha[\boldsymbol{u}_m(x,t) - \boldsymbol{u}_{im}(x,\alpha,t)] f(\alpha) d\alpha - \varphi_m \kappa \boldsymbol{u}_m(x,t) \tag{B1}$$

$$\frac{\partial \boldsymbol{u}_{im}(x,\alpha,t)}{\partial t} = \alpha[\boldsymbol{u}_m(x,t) - \boldsymbol{u}_{im}(x,\alpha,t)] - \kappa \boldsymbol{u}_{im}(x,\alpha,t) \tag{B2}$$

Inserting equation (B2) into (B1) leads to the total governing equation, written as

$$\varphi_m \frac{\partial \boldsymbol{u}_m(x,t)}{\partial t} + \varphi_{im} \int_0^\infty f(\alpha) \frac{\partial \boldsymbol{u}_{im}(x,\alpha,t)}{\partial t} d\alpha = L_t[\boldsymbol{u}_m(x,t)] - \boldsymbol{r}_k(x,t) \tag{B3}$$

in which, $\boldsymbol{r}_k(x,t)$ is the total reaction rate that integrates reactions in both mobile and immobile zones,

$$\boldsymbol{r}_k(x,t) = \varphi_m \kappa \boldsymbol{u}_m(x,t) + \varphi_{im} \int_0^\infty f(\alpha) \kappa \boldsymbol{u}_{im}(x,\alpha,t) d\alpha \tag{B4}$$

Solving equation (B2), we get the solution of components in the immobile zone, it is given by

$$\boldsymbol{u}_{im}(x,\alpha,t) = \boldsymbol{u}_{im}^0 e^{-\lambda t} + \int_0^t \alpha e^{-\lambda(t-\tau)} \boldsymbol{u}_m(x,\tau) d\tau = \boldsymbol{u}_{im}^0 e^{-\lambda t} + \alpha e^{-\lambda t} * \boldsymbol{u}_m(x,t) \tag{B5}$$

in which, $\boldsymbol{u}_{im}^0$ is the initial condition in immobile zones, $\lambda = \alpha + \kappa$ is the decay rate that accounts for both mass exchange rate and kinetic rate.

Assuming $\boldsymbol{u}_{im}^0 = 0$, then substituting equation *(B5)* into the total governing equation *(B3)*, we obtain the total governing equation with respect to component only in mobile zone, that is

$$\varphi_m \frac{\partial \boldsymbol{u}_m(x,t)}{\partial t} = L_t[\boldsymbol{u}_m(x,t)] - \varphi_{im} \left[g^0 \boldsymbol{u}_m(x,t) + \frac{\partial g(t)}{\partial t} * \boldsymbol{u}_m(x,t) + \kappa g(t) * \boldsymbol{u}_m(x,t) \right] - \varphi_m \kappa \boldsymbol{u}_m(x,t) \tag{B6}$$

in which, $g(t) = \int_0^\infty f(\alpha) \alpha e^{-\lambda t} d\alpha$ represents the memory function (Carrera et al., 1998).

To characterize the total governing equation *(B6),* we define characteristic length and characteristic transport time, written as

$$L_c = \frac{\varphi_m D}{q} \tag{B7}$$

And

$$t_c = \frac{L_c}{v} = \frac{\varphi_m^2 D}{q^2} \tag{B8}$$

In one dimensional, the characteristic length is the longitudinal dispersivity, i.e. $L_c = \alpha_L$, due to the mechanical dispersion equals to longitudinal dispersivity multiply fluid velocity, i.e. $D = \alpha_L v$.

Introducing these characteristics into equation *(B6), the dimensionless form of the total governing equation (B6) is obtained, it is given by*

$$\frac{\partial \boldsymbol{u}_m(x_D,t_D)}{\partial t_D} = \frac{\partial^2 \boldsymbol{u}_m(x_D,t_D)}{\partial x_D^2} - \frac{\partial \boldsymbol{u}_m(x_D,t_D)}{\partial x_D} - \eta \left[g^0 \boldsymbol{u}_m(x_D,t_D) + \frac{\partial g(t_D)}{\partial t_D} * \boldsymbol{u}_m(x_D,t_D) + \kappa_D g(t_D) * \boldsymbol{u}_m(x_D,t_D) \right] - \kappa_D \boldsymbol{u}_m(x_D,t_D) \tag{B9}$$

with the definition of dimensionless variables as

$$\eta = \frac{\varphi_{im}}{\varphi_m},\ t_D = \frac{t}{t_c},\ x_D = \frac{x}{L_c},\ \kappa_D = \kappa t_c,\ \alpha_D = \alpha t_c,\ \lambda_D = \lambda t_c \tag{B10}$$

Given the initial and boundary conditions,

$$\boldsymbol{u}_m(x_D, t_D = 0) = 0,\ x_D \geq 0\ \ \boldsymbol{u}_m(x_D = 0, t_D) = \boldsymbol{u},\ \boldsymbol{u}_m(x_D = \infty, t_D) = 0,\ t_D > 0 \tag{B11}$$

The solution of equation *(B9)* is obtained in the Laplace domain, that is

$$\mathscr{L}\{\boldsymbol{u}_m\} = \frac{\boldsymbol{u}}{s} exp\left\{ \left[1 - \sqrt{1 + 4(s + \kappa_D)(1 + \eta \mathscr{L}\{g\})} \right] \frac{x_D}{2} \right\} \tag{B12}$$

in which, $\mathscr{L}\{\boldsymbol{u}_m\}$ and $\mathscr{L}\{g\}$ indicate the Laplace transform of $\boldsymbol{u}_m(x_D,t_D)$ and $g(t_D)$, respectively.

References

Babey, T., de Dreuzy, J.R., Casenave, C., 2015. Multi-Rate Mass Transfer (MRMT) models for general diffusive porosity structures. Adv. Water Resour. https://doi.org/10.1016/j.advwatres.2014.12.006.

Bea, S.A., Carrera, J., Ayora, C., Batlle, F., Saaltink, M.W., 2009. CHEPROO: a Fortran 90 object-oriented module to solve chemical processes in Earth Science models. Comput. Geosci. https://doi.org/10.1016/j.cageo.2008.08.010.

Beisman, J.J., Maxwell, R.M., Navarre-Sitchler, A.K., Steefel, C.I., Molins, S., 2015. ParCrunchFlow: an efficient, parallel reactive transport simulation tool for

physically and chemically heterogeneous saturated subsurface environments. Comput. Geosci. https://doi.org/10.1007/s10596-015-9475-x.
Benson, D.A., Meerschaert, M.M., 2009. A simple and efficient random walk solution of multi-rate mobile/immobile mass transport equations. Adv. Water Resour. https://doi.org/10.1016/j.advwatres.2009.01.002.
Benson, D.A., Wheatcraft, S.W., Meerschaert, M.M., 2000. The Fractional-Order Governing Equation of Levy Motion. Water Resources Research. https://doi.org/10.1029/2000WR900032.
Berkowitz, B., Cortis, A., Dentz, M., Scher, H., 2006. Modeling Non-fickian transport in geological formations as a continuous time random walk. Rev. Geophys. https://doi.org/10.1029/2005RG000178.
Berkowitz, B., Emmanuel, S., Scher, H., 2008. Non-Fickian transport and multiple-rate mass transfer in porous media. Water Resour. Res. https://doi.org/10.1029/2007WR005906.
Berkowitz, B., Scher, H., 1998. Theory of anomalous chemical transport in random fracture networks. Phys. Rev. E. https://doi.org/10.1103/PhysRevE.57.5858.
Bilke, L., Flemisch, B., Kalbacher, T., Kolditz, O., Helmig, R., Nagel, T., 2019. Development of open-source porous media simulators: principles and experiences. Transport Porous Media. https://doi.org/10.1007/s11242-019-01310-1.
Brangarí, A.C., Fernàndez-Garcia, D., Sanchez-Vila, X., Manzoni, S., 2018. Ecological and soil hydraulic implications of microbial responses to stress – a modeling analysis. Adv. Water Resour. 116 https://doi.org/10.1016/j.advwatres.2017.11.005.
Carrera, J., Sánchez-Vila, X., Benet, I., Medina, A., Galarza, G., Guinerà, J., 1998. On matrix diffusion: formulations, solution methods and qualitative effects. Hydrogeol. J. https://doi.org/10.1007/s100400050143.
Chen-Charpentier, B., 1999. Numerical simulation of biofilm growth in porous media. J. Comput. Appl. Math. https://doi.org/10.1016/S0377-0427(98)00240-4.
Cortis, A., Berkowitz, B., 2004. Anomalous transport in "classical" soil and sand columns. Soil Sci. Soc. Am. J. https://doi.org/10.2136/sssaj2004.1539.
De Dreuzy, J.R., Rapaport, A., Babey, T., Harmand, J., 2013. Influence of Porosity Structures on Mixing-Induced Reactivity at Chemical Equilibrium in Mobile/immobile Multi-Rate Mass Transfer (MRMT) and Multiple INteracting Continua (MINC) Models. Water Resources Research. https://doi.org/10.1002/2013WR013808.
Deng, H., Spycher, N., 2019. Modeling reactive transport processes in fractures. Rev. Mineral. Geochem. 85 (1) https://doi.org/10.2138/rmg.2019.85.3.
Dentz, M., Berkowitz, B., 2003. Transport behavior of a passive solute in continuous time random walks and multirate mass transfer. Water Resour. Res. https://doi.org/10.1029/2001WR001163.
Dentz, M., Cortis, A., Scher, H., Berkowitz, B., 2004. Time behavior of solute transport in heterogeneous media: transition from anomalous to normal transport. Adv. Water Resour. https://doi.org/10.1016/j.advwatres.2003.11.002.
Dentz, M., Kang, P.K., Le Borgne, T., 2015. Continuous time random walks for non-local radial solute transport. Adv. Water Resour. https://doi.org/10.1016/j.advwatres.2015.04.005.
Donado, L.D., Sanchez-Vila, X., Dentz, M., Carrera, J., Bolster, D., 2009. Multicomponent reactive transport in multicontinuum media. Water Resour. Res. https://doi.org/10.1029/2008WR006823.
Gaebler, H.J., Eberl, H.J., 2018. A simple model of biofilm growth in a porous medium that accounts for detachment and attachment of suspended biomass and their contribution to substrate degradation. Eur. J. Appl. Math. 29 (6) https://doi.org/10.1017/S0956792518000189.
Gouze, P., Le Borgne, T., Leprovost, R., Lods, G., Poidras, T., Pezard, P., 2008a. Non-Fickian dispersion in porous media: 1. Multiscale measurements using single-well injection withdrawal tracer tests. Water Resour. Res. https://doi.org/10.1029/2007WR006278.
Gouze, Philippe, Melean, Y., Le Borgne, T., Dentz, M., Carrera, J., 2008b. Non-Fickian dispersion in porous media explained by heterogeneous microscale matrix diffusion. Water Resour. Res. https://doi.org/10.1029/2007WR006690.
Haggerty, R., Gorelick, S.M., 1995. Multiple-rate mass transfer for modeling diffusion and surface reactions in media with pore-scale heterogeneity. Water Resour. Res. https://doi.org/10.1029/95WR10583.
Haggerty, R., McKenna, S.A., Meigs, L.C., 2000. On the late-time behavior of tracer test breakthrough curves. Water Resour. Res. https://doi.org/10.1029/2000WR900214.
Haggerty, R., Wondzell, S.M., Johnson, M.A., 2002. Power-law residence time distribution in the hyporheic zone of a 2nd-order mountain stream. Geophys. Res. Lett. https://doi.org/10.1029/2002GL014743.
Hammond, G.E., Lichtner, P.C., Mills, R.T., 2014. Evaluating the performance of parallel subsurface simulators: an illustrative example with PFLOTRAN. Water Resour. Res. https://doi.org/10.1002/2012WR013483.
Iraola, A., Trinchero, P., Karra, S., Molinero, J., 2019. Assessing dual continuum method for multicomponent reactive transport. Comput. Geosci. https://doi.org/10.1016/j.cageo.2019.05.007.
Kolditz, O., Bauer, S., Bilke, L., Böttcher, N., Delfs, J.O., Fischer, T., Görke, U.J., Kalbacher, T., Kosakowski, G., McDermott, C.I., Park, C.H., Radu, F., Rink, K., Shao, H., Shao, H.B., Sun, F., Sun, Y.Y., Singh, A.K., Taron, J., Zehner, B., 2012a. OpenGeoSys: an open-source initiative for numerical simulation of thermo-hydro-mechanical/chemical (THM/C) processes in porous media. Environ. Earth Sci. https://doi.org/10.1007/s12665-012-1546-x.
Kolditz, Olaf, Görke, U.-J., Shao, H., Wang, W., 2012b. Thermo-Hydro-Mechanical-Chemical Processes in Porous Media: Benchmarks and Examples. Springer.
Kosakowski, G., Berkowitz, B., Scher, H., 2001. Analysis of field observations of tracer transport in a fractured till. J. Contam. Hydrol. https://doi.org/10.1016/S0169-7722(00)00140-6.
Le Borgne, T., Gouze, P., 2008. Non-Fickian dispersion in porous media: 2. Model validation from measurements at different scales. Water Resour. Res. https://doi.org/10.1029/2007WR006279.
Liu, P., Zhang, T., Sun, S., 2019. A tutorial review of reactive transport modeling and risk assessment for geologic CO 2 sequestration. Comput. Geosci. https://doi.org/10.1016/j.cageo.2019.02.007.
Marseguerra, M., Zoia, A., 2008. Monte Carlo evaluation of FADE approach to anomalous kinetics. Math. Comput. Simulat. https://doi.org/10.1016/j.matcom.2007.03.001.
Meysman, F.J.R., Middelburg, J.J., Herman, P.M.J., Heip, C.H.R., 2003a. Reactive transport in surface sediments. I. Model complexity and software quality. Comput. Geosci. https://doi.org/10.1016/S0098-3004(03)00006-2.
Meysman, F.J.R., Middelburg, J.J., Herman, P.M.J., Heip, C.H.R., 2003b. Reactive transport in surface sediments. II. Media: an object-oriented problem-solving environment for early diagenesis. Comput. Geosci. https://doi.org/10.1016/s0098-3004(03)00007-4.
Molins, S., Carrera, J., Ayora, C., Saaltink, M.W., 2004. A formulation for decoupling components in reactive transport problems. Water Resour. Res. https://doi.org/10.1029/2003WR002970.
Parkhurst, D.L., Appelo, C.A.J., 2013. Description of input and examples for PHREEQC version 3 — a computer program for speciation , batch-reaction , one-dimensional transport , and inverse geochemical calculations. In: U.S. Geological Survey Techniques and Methods, Book 6, Chapter A43.
Prommer, H., Barry, D.A., Zheng, C., 2003. MODFLOW/MT3DMS-based reactive multicomponent transport modeling. Ground Water. https://doi.org/10.1111/j.1745-6584.2003.tb02588.x.
Prommer, H., Barry, D., Zheng, C., 2001. PHT3D-A MODFLOW/MT3DMS based reactive multi-component transport model. MODFLOW 2001 and Other Modeling Odysseys.
Pruess, K., Narasimhan, T.N., 1985. Practical method for modeling fluid and heat flow in fractured porous media. Soc. Petrol. Eng. J.
Rapaport, A., Rojas-Palma, A., De Dreuzy, J.R., Ramirez, H.C., 2017. Equivalence of finite dimensional input-output models of solute transport and diffusion in geosciences. IEEE Trans. Automat. Control. https://doi.org/10.1109/TAC.2017.2701150.
Saaltink, M.W., Batlle, F., Ayora, C., Carrera, J., Olivella, S., 2004. RETRASO, a code for modeling reactive transport in saturated and unsaturated porous media. Geol. Acta. https://doi.org/10.1344/105.000001430.
Saaltink, Maarten W., Ayora, C., Carrera, J., 1998. A mathematical formulation for reactive transport that eliminates mineral concentrations. Water Resour. Res. https://doi.org/10.1029/98WR00552.
Saaltink, Maarten W., Carrera, J., Ayora, C., 2001. On the behavior of approaches to simulate reactive transport. J. Contam. Hydrol. https://doi.org/10.1016/S0169-7722(00)00172-8.
Salamon, P., Fernàndez-Garcia, D., Gómez-Hernández, J.J., 2006. Modeling mass transfer processes using random walk particle tracking. Water Resour. Res. https://doi.org/10.1029/2006WR004927.
Schumer, R., Benson, D.A., Meerschaert, M.M., Baeumer, B., 2003. Fractal mobile/immobile solute transport. Water Resour. Res. https://doi.org/10.1029/2003WR002141.
Silva, O., Carrera, J., Dentz, M., Kumar, S., Alcolea, A., Willmann, M., 2009. A general real-time formulation for multi-rate mass transfer problems. Hydrol. Earth Syst. Sci. https://doi.org/10.5194/hess-13-1399-2009.
Soler-Sagarra, J., Luquot, L., Martínez-Pérez, L., Saaltink, M.W., De Gaspari, F., Carrera, J., 2016. Simulation of chemical reaction localization using a multi-porosity reactive transport approach. Int. J. Greenhouse Gas Contr. https://doi.org/10.1016/j.ijggc.2016.01.026.
Steefel, C.I., Appelo, C.A.J., Arora, B., Jacques, D., Kalbacher, T., Kolditz, O., Lagneau, V., Lichtner, P.C., Mayer, K.U., Meeussen, J.C.L., Molins, S., Moulton, D., Shao, H., Šimůnek, J., Spycher, N., Yabusaki, S.B., Yeh, G.T., 2015. Reactive transport codes for subsurface environmental simulation. Comput. Geosci. https://doi.org/10.1007/s10596-014-9443-x.
Steefel, C.I., Lasaga, A.C., 1994. A coupled model for transport of multiple chemical species and kinetic precipitation/dissolution reactions with application to reactive flow in single phase hydrothermal systems. Am. J. Sci. https://doi.org/10.2475/ajs.294.5.529.
Tiwari, S.K., Bowers, K.L., 2001. Modeling biofilm growth for porous media applications. Math. Comput. Model. 33 (1–3) https://doi.org/10.1016/S0895-7177(00)00246-6.
Wang, P.P., Zheng, C., Gorelick, S.M., 2005. A general approach to advective-dispersive transport with multirate mass transfer. Adv. Water Resour. https://doi.org/10.1016/j.advwatres.2004.10.003.
Willmann, M., Carrera, J., Sánchez-Vila, X., 2008. Transport upscaling in heterogeneous aquifers: what physical parameters control memory functions? Water Resour. Res. https://doi.org/10.1029/2007WR006531.
Willmann, M., Carrera, J., Sanchez-Vila, X., Silva, O., Dentz, M., 2010. Coupling of mass transfer and reactive transport for nonlinear reactions in heterogeneous media. Water Resour. Res. https://doi.org/10.1029/2009WR007739.
Zhang, Y., Benson, D.A., Baeumer, B., 2007. Predicting the tails of breakthrough curves in regional-scale alluvial systems. Ground Water. https://doi.org/10.1111/j.1745-6584.2007.00320.x.
Zinn, B., Meigs, L.C., Harvey, C.F., Haggerty, R., Peplinski, W.J., Von Schwerin, C.F., 2004. Experimental visualization of solute transport and mass transfer processes in two-dimensional conductivity fields with connected regions of high conductivity. Environ. Sci. Technol. https://doi.org/10.1021/es034958g.